

The effect of blood inflow and B_1 inhomogeneity on the arterial input function in 3-D DCE-MRI

C. Roberts¹, R. A. Little¹, S. Zhao¹, Y. Watson¹, D. L. Buckley¹, and G. J. Parker¹

¹Imaging Science and Biomedical Engineering, The University of Manchester, Manchester, Greater Manchester, United Kingdom

Introduction In early-stage clinical trials of anti-vascular and anti-angiogenic therapies, dynamic contrast-enhanced MRI (DCE-MRI) and kinetic modeling can be used to extract tumor microvascular parameters. A 3-D axially-acquired volume of DCE-MRI data containing the tumor volume, and a major vessel for measurement of an arterial input function (AIF, $C_p(t)$) is often acquired. An individually-measured AIF is always desirable over an assumed AIF, but must be both accurate and reproducible as end-point summary parameters are heavily influenced by the AIF. These are challenging conditions to meet due to many contributing factors to errors in a AIF measurement (1,2). Errors due to blood inflow and B_1 inhomogeneity across the imaging slab mean that the location within the imaging volume used for AIF measurement is critical. We quantify these errors on the accuracy of $C_p(t)$ using a combination of computer simulations, flow phantom, B_1 mapping, and clinical *in vivo* measurements in order to determine the validity of AIF measurements in 3-D DCE-MRI.

Methods Flow Phantom: A pump-driven MR compatible flow apparatus was placed in the bore of a 1.5 T Philips Intera (Best, Netherlands) scanner (see ref (3) for detailed description) which circulated Omniscan-doped (GE Healthcare) water at a flow rate of 57 cm/s, which is comparable to aortic flow rates *in vivo*. Baseline T_1 was measured using a 3-D Fast Field Echo (T1-FFE/SPGR) sequence with the following parameters: 2°, 10° and 20° flip angles, TR/TE = 4.0/1.02 ms, FOV = 165 mm², matrix = 128², slices = 25, thickness = 4 mm. The dynamic image acquisition used the same parameters with a flip angle of 20°, 42 dynamic timepoints and a temporal resolution of 4.97 s. A 1 ml bolus of 0.5 mmol/ml Omniscan mixed with black food dye (Supercolor, Leeds, UK) (1:1 ratio) was administered at a rate of 2 ml/sec. A region of interest (ROI, consisting of 16 pixels minimum) was defined in the axial plane of the tubing for each slice in the volume (see Fig. 1). Baseline T_1 and M_0 was determined using a non-linear fitting routine. AIFs were extracted for each slice and converted to $C_p(t)$ using the standard relationship to $1/T_1(t)$ (4). These AIFs were compared against a "gold-standard" AIF previously reported using this MR phantom (3). A 16-point B_1 mapping sequence was also implemented using the same gradients, RF pulse shape, FOV, slices = 10, thickness = 10 mm, with nominal flip angles of 0°, 150° and then every 15° increments to 360° (5). The effective flip angle (FA_{eff}) after accounting for B_1 variation was mapped at each slice (Fig. 1 and 2a).

Simulations: To test the errors due to blood in-flow and B_1 inhomogeneity we simulate the generation of the steady-state signal for a 3D SPGR acquisition. We simulate a baseline T_1 measurement (incorporating the effective flip angle determined from the B_1 mapping sequence) using identical acquisition parameters and fitting routine as above. AIFs were simulated for each slice in the volume. Blood flow was assumed to be perpendicular to the volume and non-pulsatile.

In-vivo DCE-MRI data: 15 patients with advanced abdominal and colorectal cancer (and with the aorta captured in the whole imaging volume) who were enrolled in a Phase II DCE-MRI clinical trial to assess the efficacy of a novel anti-vascular drug were retrospectively investigated. Each patient undertook 5 separate DCE-MRI scans on different occasions, with identical nominal flip angle, TR/TE as stated above, including a baseline volume variable flip angle gradient-echo T_1 measurement followed by 75 volumes, with a temporal resolution of 4.97 s. On the sixth dynamic timepoint, 0.1 mmol/kg of body weight of 0.5 mmol/ml Omniscan was administered through a Spectris power injector (Medrad Inc.) at a rate of 3 ml/s followed by an equal volume of saline flush also at 3 ml/s.

Analysis: The area under the AIF (AUC_{AIF}) at each slice location was computed using trapezoidal integration to provide a simple measure to allow comparison of AIFs between simulations, phantom measurements, and *in vivo*.

Results The variation in flip angle determined in the flow phantom (Fig. 1) shows that there are large under-estimations of the true flip angle towards the edges of the imaging volume and slight over-estimations in the centre of the imaging volume in our ROI (Fig. 2a), as would be expected due to dielectric and volume selection pulse profile effects. The AIF measurements from the phantom and *in vivo* data are in close agreement with the simulated values (Fig. 2b,c); all three show slice location-dependant errors due to B_1 inhomogeneity and inflow effects. Specifically, the first 1-8 slices receiving fresh inflowing blood suffer an over-estimation of AIF amplitude. Similarly there is an over-estimation in the latter 2-3 slices due to the B_1 fall-off demonstrated in Fig. 2a.

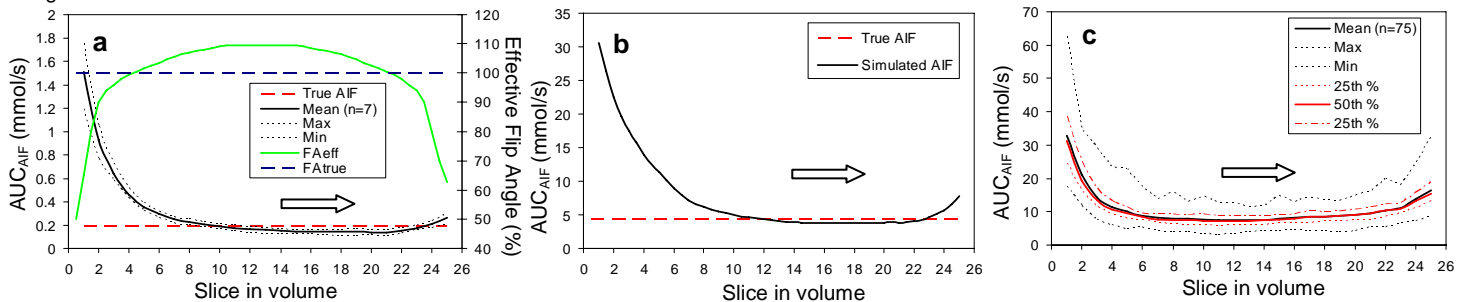


Figure 2: The area under the AIF curve (AUC_{AIF}) calculated for AIFs measured in the MR flow phantom (a), computer simulations (b) and from 15 patients, representing 75 AIFs per slice (c). Block arrow indicates direction of flow. Effective and true flip angle (%) as measured in the MR phantom are shown in (a).

Discussion & Conclusions The quantification of AIF errors in 3D axial DCE-MRI is demonstrated by use of an MR flow phantom and our "gold standard" AIF (3), computer simulations and *in vivo* data. Systematic over-estimations of AIF amplitude at the edges of the imaging volume are due to a combination of fresh inflowing spins in the first 1-8 slices (1-32 mm) and B_1 inhomogeneity – this trend is demonstrated across all 3 experiments. More importantly, we have shown that a measurement of the AIF in a mid-volume location ensures that the effects of blood inflow and B_1 inhomogeneity are negligible.

References 1. Henderson E *et al.* Magn Reson Imaging 1998;16(9):1057-1073. 2. Roberts C *et al.* Magn Reson Med 2006;56(3):611-619. 3. Little R *et al.* 2007; Proceedings of the 15th Annual ISMRM. p 2985. 4. Li KL *et al.* J Magn Reson Imaging 2000;12(2):347-357. 5. Vaughan JT *et al.* Magn Reson Med 2001;46(1):24-3